Extreme Solar Storms and the Quest for Exact Dating with Radiocarbon

Authors: T. J. Heaton[1]*, E. Bard[2], A. Bayliss[3], M. Blaauw[4], C. Bronk Ramsey[5], P. J. Reimer[4], C. S. M. Turney[6,7], I. Usoskin[8]

Affiliations:

[1]Department of Statistics, School of Mathematics, University of Leeds, Leeds LS2 9JT, UK.

[2]CEREGE, Aix-Marseille University, CNRS, IRD, INRAE, Collège de France, Technopole de l'Arbois BP 80, 13545 Aix en Provence Cedex 4, France.

[3]Historic England, 25 Dowgate Hill, London, EC4R 2YA, UK.

[4]The [14]CHRONO Centre for Climate, the Environment and Chronology, Geography, Archaeology and Palaeoecology, School of Natural and Built Environment, Queen's University Belfast BT7 1NN, UK.

[5]Research Laboratory for Archaeology and the History of Art, University of Oxford, 1 South Parks Road, Oxford OX1 3TG, UK.

[6]Institute of Sustainable Futures, Division of Research, University of Technology Sydney, Ultimo, NSW 2007, Australia

[7]Chronos [14]Carbon-Cycle Facility, University of New South Wales, Sydney, NSW 2052, Australia

[8]Space Physics and Astronomy Research Unit and Sodankylä Geophysical Observatory, University of Oulu, 90014 Oulu, Finland

*Correspondence to: t.heaton@leeds.ac.uk.

ORCID:

T J Heaton ORCID: https://orcid.org/0000-0002-9994-142X

E Bard ORCID: https://orcid.org/0000-0002-7237-8622

A Bayliss ORCID: https://orcid.org/0000-0003-2782-1979

M Blaauw ORCID: https://orcid.org/0000-0002-5680-1515

C Bronk Ramsey ORCID: https://orcid.org/0000-0002-8641-9309

P J Reimer ORCID: https://orcid.org/0000-0001-9238-2146

C S M Turney ORCID: https://orcid.org/0000-0001-6733-0993

I Usoskin ORCID: https://orcid.org/0000-0001-8227-9081

Abstract/Summary:

Radiocarbon (^{14}C) is essential for creating chronologies to study the timings and drivers of pivotal events in human history and the Earth system over the last 55,000 years. It is also fundamental as a proxy for investigating solar processes, including the Sun's potential for extreme activity. Until now, fluctuations in past atmospheric ^{14}C levels have limited the dating precision possible using radiocarbon. However, the recent discovery of solar super-storms known as extreme solar particle events (ESPEs) has driven a series of advances with the potential to transform the calendar age precision of radiocarbon dating. Organic materials containing the unique ^{14}C ESPE signatures can now be dated to annual precision. In parallel, the search for further storms using high-precision annual ^{14}C measurements has revealed fine-scaled variations in radiocarbon that can improve calendar age precision, even in periods that lack ESPEs. Furthermore, the newly identified ^{14}C fluctuations provide unprecedented insight into solar variability and the carbon cycle. Here, we review the current state-of-knowledge and share our insights on these rapidly developing, diverse research fields. We identify links between the radiocarbon community, archaeology, solar physics, and Earth science to stimulate transdisciplinary collaboration, and propose how users may take advantage of these recent developments.

Perspective Layout

Since its existence was confirmed in 1940[1], radiocarbon has been both a cornerstone for dating the past 55,000 years and a fundamental tracer of Earth system processes. This perspective draws together recent developments across multiple disciplines that offer novel insights into the archaeological, Earth, and space sciences. We discuss how the discovery of so-called 'Miyake' events caused by extreme solar particle events (ESPEs) has provided new opportunities for more precise radiocarbon calibration, and stimulated research programmes to measure past ^{14}C levels at annual resolution. We summarise how scientists can use ESPEs directly to obtain exact dating using radiocarbon, and how they can leverage fine-scale ^{14}C variations identified by the wider annual measurement programmes for calibration more broadly. We also survey the novel insights that ESPEs and consequent high-precision annual ^{14}C measurements have provided regarding space weather and the global carbon cycle, and describe areas where further research is required to gain the greatest value from radiocarbon.

Introduction to Radiocarbon

The ca. 5700-year half-life of the radioactive isotope of carbon (radiocarbon or ^{14}C), and the ubiquitous nature of carbon in the biogeosphere, makes it uniquely useful as a scientific tool to study the last 55,000 years: both as the primary clock to measure time for archaeologists and environmental scientists, and to probe key Earth system processes[2,3].

Radiocarbon dating[4,5] is based upon the principle that, while an organism is alive, it exchanges carbon with its surroundings and so will have a ratio of ^{14}C to stable carbon that is in equilibrium with that of its local environment; a similar situation also arises in some

geological processes such as the growth of speleothems. Once exchange ceases, for example when an organism dies, the stable carbon incorporated into well-preserved chemical components will remain constant, but the amount of ^{14}C will halve every ca. 5700 years. Beyond ten half-lives (ca. 60,000 years) insufficient ^{14}C remains to be measured reliably with current methods.

If the ^{14}C concentration (ratio of ^{14}C to stable carbon) in the various reservoirs of the carbon cycle had been constant over time, obtaining a precise calendar age from radiocarbon dating would be straightforward. However, the ^{14}C concentration has varied considerably over time and differs according to the carbon reservoir (e.g., atmosphere or ocean) under study. These past fluctuations mean that all radiocarbon age measurements need to be adjusted to account for the ^{14}C concentration when the sample stopped carbon exchange. This adjustment is known as radiocarbon calibration.

Calibrating a ^{14}C measurement into an accurate calendar date requires comparison against reference material of known calendar age (tree-rings dated by dendrochronology) or other independently-dated ^{14}C records (such as stalagmites, corals, and lacustrine and marine sediments)[3]. These reference materials are combined into calibration curves that provide estimates of the ^{14}C concentration of a sample that stopped exchanging in any individual calendar year[6–8]. To calibrate a sample of unknown age, we calculate which calendar dates are consistent with the sample's observed ^{14}C concentration. This is typically achieved via a Bayesian approach (Figure 1 and SI video 1). Calibration leads to calendar age estimates that are uncertain, and have potentially complex, asymmetric, and multimodal probability distributions. The requirement for calibration is one of the main confounding factors in ^{14}C dating and many important archaeological debates, such as the date of the Minoan eruption of Thera in the 2nd millennium BC, hinge on these calendar age probability distributions[9–11].

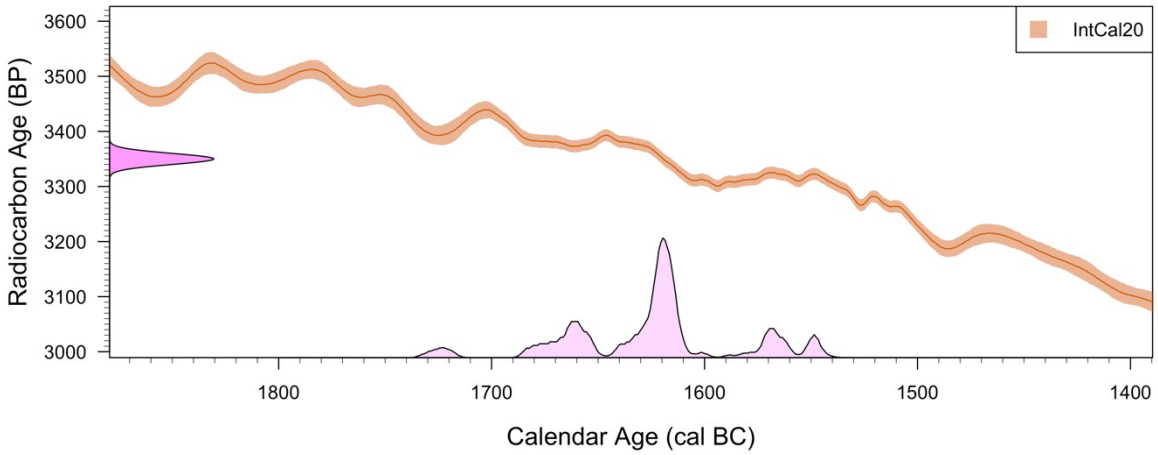

Figure 1 Radiocarbon calibration of the Minoan eruption of Thera. The average of multiple key samples[9,11] indicate a ^{14}C age of 3350 ± 10 BP. To calibrate this ^{14}C determination, shown in dark magenta on the y-axis, we estimate which calendar dates are compatible with it. The IntCal20 calibration curve[6] (with 1σ-uncertainties) is shown in orange, and the compatible

calendar dates are shown as a probability distribution along the x-axis in light magenta. For an animation, see SI video 1.

Calibration and Calendar Age Precision

The need for calibration means that the calendar age precision produced from radiocarbon dating arises from two distinct components. Firstly, the measurement precision of the ^{14}C content of the sample; and secondly the calendar age uncertainty introduced through the calibration process. Improvements in the former without consideration of how to reduce the latter offer only limited progress in increasing calendar age precision. For some ^{14}C users, typically those able to obtain just a single ^{14}C determination, the imprecision introduced through calibration may be irreducible. However, for those with access to multiple potential ^{14}C samples, careful consideration of how and what they choose to measure and calibrate offers substantial opportunities to reduce their final calendar age uncertainties.

Archaeologists have been quick to embrace the potential for more precise chronologies by incorporating independent information, either on relationships between the ^{14}C samples or with external chronologies, during calibration[12,13]. The routine application of Bayesian chronological modelling has led to the development of a step-by-step process to enable the selection of suites of samples for dating that can be interpreted together in formal statistical models[14]. Currently, relative dating known from stratigraphy, either from archaeology or environmental records, is the most widely used information incorporated into chronological models, although other kinds of sequence, such as artefact typology or seriation, are also used. This can be supplemented by tie-points provided, for example, by volcanic tephra[15]. Until recently, the decadal resolution of most of the data used to construct calibration curves has however been a limitation on the types of independent archaeological and environmental information that can be used in chronological modelling[16]. The discovery of ESPEs has changed this.

Atmospheric $^{14}C/^{12}C$ Variations

The variations in past atmospheric levels of ^{14}C that necessitate calibration are a consequence of both changes in the rate of production over time and rearrangements in the global carbon cycle. Consequently, discoveries in the ^{14}C record which lead to improvements in radiocarbon calibration also enable key insights in a broad range of other scientific fields.

Natural production of ^{14}C predominantly occurs in the lower stratosphere and upper troposphere driven by galactic cosmic rays (GCRs). These incoming GCRs initiate a cascade of nuclear collisions, eventually generating neutrons which then react with atmospheric nitrogen to produce ^{14}C. The number of GCRs which reach the atmosphere is modulated by the strength of the solar magnetic field and the geomagnetic field. Both partially shield Earth from cosmic radiation. When solar activity is high, and/or the geomagnetic field is strong, fewer GCRs reach Earth, leading to lower ^{14}C production rates and vice versa. Variations in the rate of ^{14}C production due to solar activity tend to operate on short-to-moderate time scales (decadal to centennial); while those due to changes in the geomagnetic field generally operate on much longer, centennial to millennial, timescales.

Until recently, no abrupt changes had been identified in the ^{14}C record and it was believed that the cosmic-ray flux impinging on Earth varied only gradually in response to heliospheric and geomagnetic modulation[17–19]. Consequently, measurement of reference ^{14}C material at annual resolution was seen as a low priority. However, in 2012, analysis of a Japanese cedar identified an unexpected 12‰ increase in atmospheric $\Delta^{14}C$ (a decrease of >100 ^{14}C yr) over the course of a single year AD 774–775[20]. Such an abrupt increase in ^{14}C levels required an entirely unprecedented spike in ^{14}C production to have occurred during that year – almost four times the yearly average[21].

Further analysis identified that the cause of this ^{14}C jump was an extreme solar storm an order-of-magnitude greater in size than any previously estimated[22]. Such a storm would have created a massive short-term burst of energetic solar particles (an ESPE) that led to a huge spike in ^{14}C production.

Impact of the Discovery of ESPEs

The occurrence of similar ESPEs today could have disastrous impacts on our telecommunications, electricity grids, and satellite systems[23,24]. Understanding the frequency of such events and their possible size is therefore essential to prepare and build resilience into these systems. Since detailed instrumental measurements of the Sun's behaviour are only available for the last few decades, during which no ESPEs have occurred, we are required to use the imprint they leave in cosmogenic isotope records. The discovery of the AD 774 ESPE initiated new and extensive programmes to measure ^{14}C in tree-rings at annual resolution and high precision throughout the Holocene. These programmes have important implications for solar physics, enhancing our understanding of the Sun and space weather. They also provide new opportunities for those seeking to calibrate radiocarbon determinations.

The ^{14}C signatures left by ESPEs are unique. If one can obtain ^{14}C samples from consecutive calendar years that bracket the ESPE (for example, by measuring individual growth-rings within timbers) calibration to the exact year is possible. This step-change in the precision obtainable through radiocarbon dating has the potential to extend the reach of the radiocarbon method into historical and other problems which require exact dating. Most immediately, such exact dating will be of relevance to archaeologists. However, several fields of Earth sciences crucially also need high-precision dating when dealing with rare, but dramatic, events like earthquakes and tsunamis[25], extreme weather events such as hurricanes[26], or rainfall and flood events[27] all of which may have varied in strength and frequency in the past. Confirming the correct identification of at least a few singular events in distant archives would demonstrate the reliability of available records in this growing field of paleo-extreme events.

While those studying periods lacking in ESPEs (or without suitable items to bracket the ESPE) may not be able to obtain exact dating using ^{14}C, they can still take advantage of the increased resolution in radiocarbon calibration curves enabled by the annual ^{14}C measurement programmes. Such fine-scaled understanding of atmospheric ^{14}C structure allows relative dating information from shorter ^{14}C sequences and/or shorter-lived ^{14}C samples to be used more effectively and reliably in statistical models. Harnessed optimally during calibration,

this indirect consequence of the search for ESPEs will improve the dating accuracy and precision of ^{14}C more broadly.

Notation

When discussing ^{14}C, we denote conventional radiocarbon ages as BP (radiocarbon years before present)[28]. Calendar years (e.g., those derived from dendrochronology or historical events) are expressed as AD/BC (or CE/BCE), while calibrated radiocarbon measurements are expressed either as cal BC/AD or as cal BP (calibrated years before present). Here, '*present*' is defined as the year AD 1950, so that, e.g., 10 cal BP = cal AD 1940. When discussing inference on the Earth system, we use $\Delta^{14}C$ which denotes depletion or enrichment of the (age-corrected and fractionation-corrected) $^{14}C/^{12}C$ ratio relative to an international standard expressed in per mil (‰)[29].

We define an ESPE[30,31] as a solar particle storm which can be statistically-significantly resolved (at the 3σ level) in the annual cosmogenic-isotope data and where the flux of particles with kinetic energy >200 MeV time-integrated over the entire event (the F_{200} particle fluence) exceeds 10^9 cm^{-2}.

Recent Advances in ^{14}C and Calibration

Extreme Solar Particle (Miyake) Events

Initially, the AD 774 "Miyake" spike was proposed to be the consequence of a nearby supernova, however, it was soon shown that the only plausible cause was the Sun, specifically an ESPE with an enormous flux of solar energetic particles (SEPs) producing a spike of cosmogenic isotopes in the Earth's atmosphere[22]. This solar event was later confirmed by similar peaks in $\Delta^{14}C$ from other trees around the world, as well as in other cosmogenic isotopes ^{10}Be and ^{36}Cl measured in ice cores[21,32]. The use of different isotopes and sophisticated modelling made it possible to identify that the event had likely occurred during the Northern Hemispheric (NH) summer of AD 774. The reconstructed SEP energy spectrum[21,33] appeared similar to 'normal' solar particle storms but several orders of magnitude higher in flux.

While the identification of these huge spikes in ^{14}C production has enabled ^{14}C calibration at annual precision, studying the spikes themselves is also key to better understand the behaviour of the Sun and the potential risks that it poses to Earth and our technological society. The long-term behaviour of the Sun is poorly documented. Direct observational measurements of sunspots have only been recorded for a few centuries[34] and more detailed instrumental measurements for only a few decades. The largest, directly-observed, solar storm occurred on 1-2 September AD 1859 (the 'Carrington Event') and led to widespread disruption including the destruction of telegraph machines and an aurora so bright that it seemed the Sun had begun to rise[35]. However, so far, no identifiable increase in either $\Delta^{14}C$ or ^{10}Be has been detected for this Carrington Event (although a transient high-latitude offset in $\Delta^{14}C$ has been tentatively proposed a couple of years after the event[36]). The AD 774 Miyake Event was an entire order-of-magnitude greater in size, making understanding the risks of ESPEs even more critical.

The discovery of the first Miyake event stimulated solar physics research and initiated a race for ^{14}C measurement programmes at annual resolution to identify further ESPEs and investigate the potential for other fine-scaled solar behaviour. This work has been facilitated by advances in AMS instrumentation[37–39] meaning high-precision ^{14}C measurements (< 2‰ in $\Delta^{14}C$, ±16 BP) on samples containing just a few mg of carbon can now be achieved much more efficiently. So far, five ESPEs have been confirmed based upon a comparison of multiple radionuclides (7176 BC, 5259 BC, 660 BC, AD 774 and AD 993) along with four further potential candidates (12,350 BC, 5410 BC, AD 1052, AD 1279) that are still to be confirmed[21,40–46].

Annual Resolution ^{14}C Measurements

While ^{14}C measurements on known-age single tree-rings have been available for use in ^{14}C calibration for decades, they focussed only on the last few centuries, and their extension further back in time was not seen as urgent for calibration[47]. Most of the reference ^{14}C datasets used in calibration curve construction were instead measurements of 5-, 10-, or 20-year blocks of tree-rings. The new measurement programmes have generated huge numbers of annual tree-ring ^{14}C measurements, although primarily from the Northern Hemisphere.

Even in periods without ESPEs, they reveal short-term fluctuations in ^{14}C concentrations that had been obscured in the legacy multi-year measurements. Such information can be used by anyone wishing to calibrate.

The IntCal20 Northern Hemisphere curve[6] is now based entirely on tree-ring measurements from 13,910–0 cal BP. In this period, it draws upon 10,713 ^{14}C measurements from tree-ring samples. Of these 5866 now correspond to single-year measurements covering 2734 individual calendar years (Figure 2A). Currently, these new annual-resolution sections of calibration curve tend to concentrate on hot-topic periods: specifically, the most recent millennium, the two original Miyake events, the date of the Minoan eruption of Thera (Figure 1 and 2B), and the Younger Dryas climatic event. However, IntCal20 does not include the most recently issued datasets[41,42,44,45] and coverage of the Holocene with annual ^{14}C measurements is expected to increase substantially.

The current SHCal20 Southern Hemisphere curve[8] has a lot fewer annual ^{14}C measurements upon which to draw. It is based upon 2091 direct ^{14}C measurements of tree-rings, covering just four distinct periods: 2140–0, 3520–3453, 3608–3590, and 13,140–11,375 cal BP. Of these, only 262 correspond to single-year ^{14}C measurements covering just 150 individual calendar years. The remainder of the SHCal20 curve is based on modelling (applying a 36 ± 27 ^{14}C yr interhemispheric offset, to older ages, from IntCal20). Consequently, the SHCal20 curve must be considered with care if using short-term ^{14}C fluctuations as they have mostly been inferred from the NH data.

Beyond 13,910 cal BP the resolution of all calibration curves is much lower due to current limitations on our ^{14}C archives. Here the calibration curves are predominantly reliant upon measurements from Hulu Cave stalagmites[48,49] which are smoothed due to the various natural processes involved. However, new tree ring archives are becoming available[45,50,51] providing hope that annual-resolution calibration curves based on tree-rings will soon extend further into the past.

Calibration Curve Construction

The IntCal calibration curves[6–8] combine all reference ^{14}C measurements that pass selection criteria[52]. This includes both single-year and multi-year measurements, with the latter modelled as such. The current IntCal20 and SHCal20 curves are generated using Bayesian splines – generating a set of individual posterior realisations which are then summarised[53]. The final curves aim to take account of, and represent, the over-dispersion observed in ^{14}C measurements within a hemisphere (i.e., that observed ^{14}C determinations in any calendar year are more widely spread than expected based upon their quoted laboratory uncertainties).

The current construction methods are designed to permit more detail to be retained in time periods with large volumes of single-year measurements (Figure 2B). However, they still implicitly model the underlying processes as smooth over time. Consequently, over ESPEs, they tend to smooth out the ^{14}C production spikes so that the increases in $\Delta^{14}C$ (Figure 2C and 2D) occur over more than a single year (although this is also partially a consequence of the

seemingly different timing of some of the events in different set of trees – see later Case Study II).

As a result of this smoothing, those seeking exact calibration over ESPEs have predominantly used the direct mean of annual ^{14}C measurements from a reduced set of locations[54] in place of the IntCal curves. These direct-mean curves only cover short time periods and do not consider overdispersion. To demonstrate what potentially could be achieved if the international curves were modified to enable sharp ESPE discontinuities, we present a tentative *MiyakeCal* curve over the AD 774 event (Figure 2C and 2D). *MiyakeCal* uses the same methodology as IntCal20, but allows an additional jump in $\Delta^{14}C$ from AD 774–775 to be superimposed on the smooth spline processes.

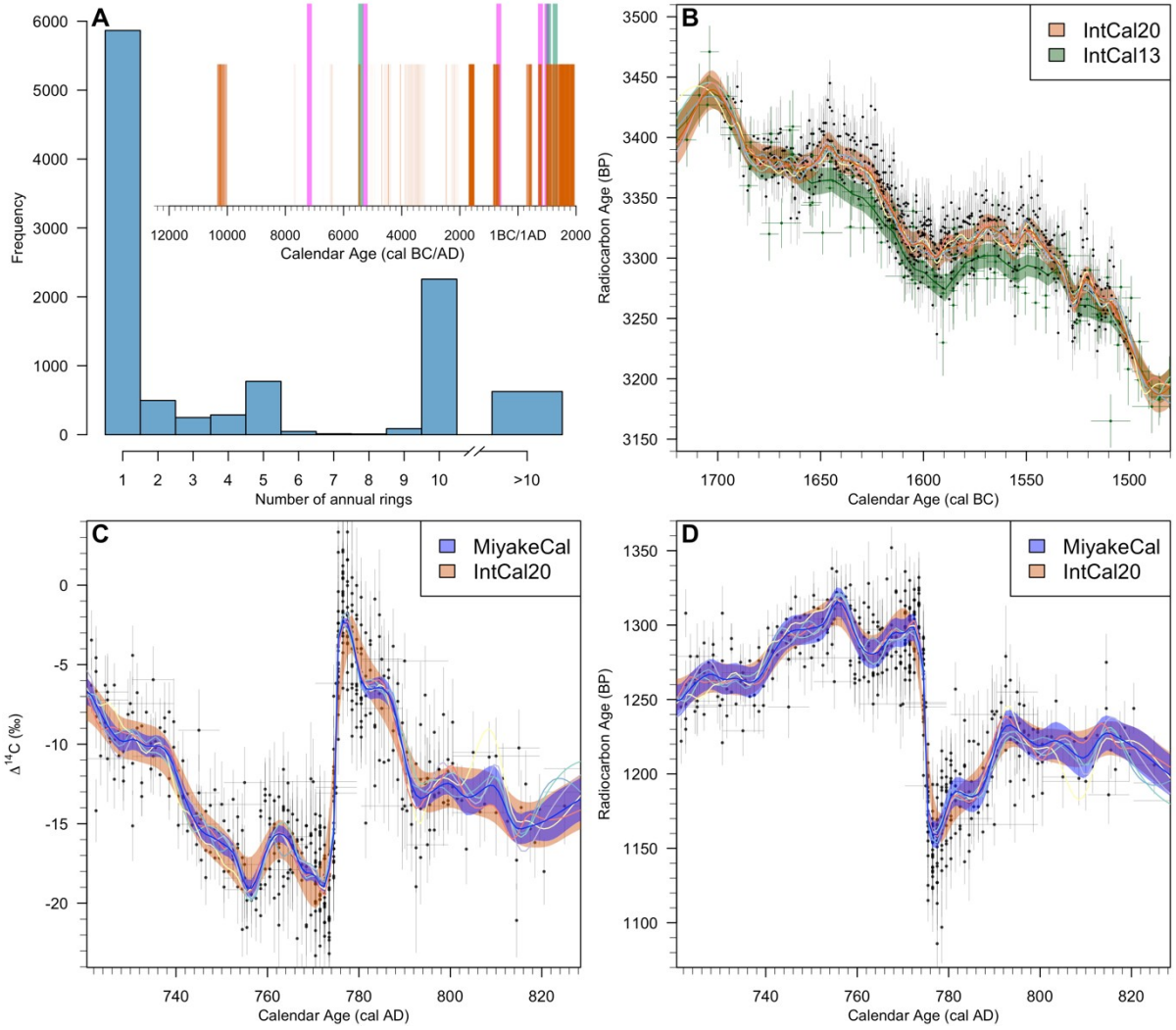

Figure 2: Panel A - Distribution of the block sizes in the tree-ring ^{14}C measurements used for the IntCal20 curve[6] back to 13,910 cal BP. Before the discovery of the AD 774 ESPE, most reference ^{14}C samples were multi-annual tree-rings (often 10-yr blocks). Inset shows the calendar years with annual resolution ^{14}C data (orange vertical bars), together with the confirmed (magenta) and potential (green) ESPEs in the Holocene. Panel B: The increased annual detail available with IntCal20[6] compared to IntCal13[55] during the 2nd millennium BC. Panel C: The IntCal20 curve over the AD 774 ESPE plotted in $\Delta^{14}C$. This is shown alongside the preliminary MiyakeCal curve designed to better represent the ESPE's abrupt increase in

^{14}C production. Panel D: IntCal20 and MiyakeCal plotted in radiocarbon age. For IntCal20 (panel B) and MiyakeCal (panels C–D), a sample of posterior curve realizations are plotted (variously-coloured lines), together with the summarized posterior mean (solid orange/blue line) and 1σ-intervals (shaded orange/blue). All observations (black dots) are shown with 1σ error-bars on the ^{14}C axis, the horizontal bars represent the individual years represented in (multi-annual) measurements.

Improving ^{14}C calibration

Exact Dating by ESPE Wiggle-Matching

Almost immediately after the discovery, it was realised that the substantial jumps in ^{14}C production during ESPEs could provide exact calendar age precision from ^{14}C calibration if it was possible to find timber with growth rings that spanned an event. Measurement of ^{14}C in consecutive annual samples to discover the corresponding jump in ^{14}C concentration allows exact identification of the ESPE's calendar year. Counting from this growth-ring to the final waney-edge in the timber then provides the precise year in which the tree was felled. This process is known as ^{14}C wiggle-matching and can be implemented in two different ways, see Case Study I.

The first application of these ideas, undertaken in 2014, provided an exact date for felling of timber used in the Holy Cross chapel of the St. John the Baptist convent, a UNESCO world heritage site in Val Müstair, Switzerland[56]. This has been followed by further examples[57–63] including the exact anchoring of the stratigraphy of a Viking Age trade centre[61], identification of the precise year in which Vikings were present in N. America[62], and evidence for a compound earthquake involving simultaneous ruptures across two fault zones near Seattle[63].

The principle has the potential to be extended to any ESPE of sufficient magnitude. Currently, applications have focussed on identification of the AD 774 or AD 993 events, although a recent study has proposed using the 5259 BC ESPE to date a floating Neolithic tree-ring chronology in Dispilio, Northern Greece[64]. Users of the AD 993 event must however proceed with care, as the exact timing of this ESPE's ^{14}C signature in tree-rings does not appear globally consistent (see Case Study II) and the choice of ^{14}C reference data is crucial to obtain reliable exact ^{14}C calibration.

Leveraging Annual ^{14}C Calibration Curves

For archaeologists and environmental scientists not studying periods with an ESPE, or who lack preserved wood on their sites, it is still possible to exploit the new annual-resolution detail in ^{14}C calibration curves. Sampling strategies that allow stratigraphic and relative calendar information to be incorporated into calibration are key. Since the advent of routine chronological modelling, the identification and inclusion of sequences of samples that can be ordered independently has been essential for maximising dating precision. Annual resolution calibration datasets mean shorter sequences, and sequences of short-lived samples, may now be included in models more effectively. This can substantially increase calendar age precision, particularly on calibration plateaus.

Instead of submitting a single sample from a seed, one may aim to calibrate a sequence obtained from a charcoal fragment[65]. Short wiggle-matches may also be obtained from timbers in historic or protohistoric buildings unsuitable for dendrochronology[66–68]. Studies of human bone provide a further example, although modelling is complicated by the potential for dietary reservoir effects[69] and bone collagen turnover[70] where additional research is sorely needed[71]. Sampling a single tooth in several individuals, who died at the same time, but were of different ages when they died, enables a relative sequence of samples to be elicited from a

group of burials[72]. Differences in the formation times of different bones in a human skeleton, such as the petrous and rib, can also be used to produce a sequence of ^{14}C measurements through a dated individual[73]. Case Study III combines the sampling of both teeth and bone from multiple individuals into a sequence of six ^{14}C determinations with varying calendar age gaps[74,75]. Increasingly, studies of ancient DNA are not only providing phylogenetic trees[76], but kinship relationships between individuals[77]. These relationships can also provide short sequences for chronological models, either based on the degree of kinship[78] or on reconstructed pedigrees[77,79].

Case Study I

Bayesian wiggle-matching vs χ^2 testing: The timber lake-fortress in Lake Āraiši

There are two approaches to calibrating ^{14}C sequences which we illustrate using the timber lake-fortress in Lake Āraiši, Latvia[60]. Single-year samples for 14 consecutive annual rings were obtained for a spruce timber recovered from the log-platform during excavation (Figure I-A). These annual measurements contain the AD 774–775 signature with a drop of over 100 ^{14}C yr observed over the course of a single calendar year.

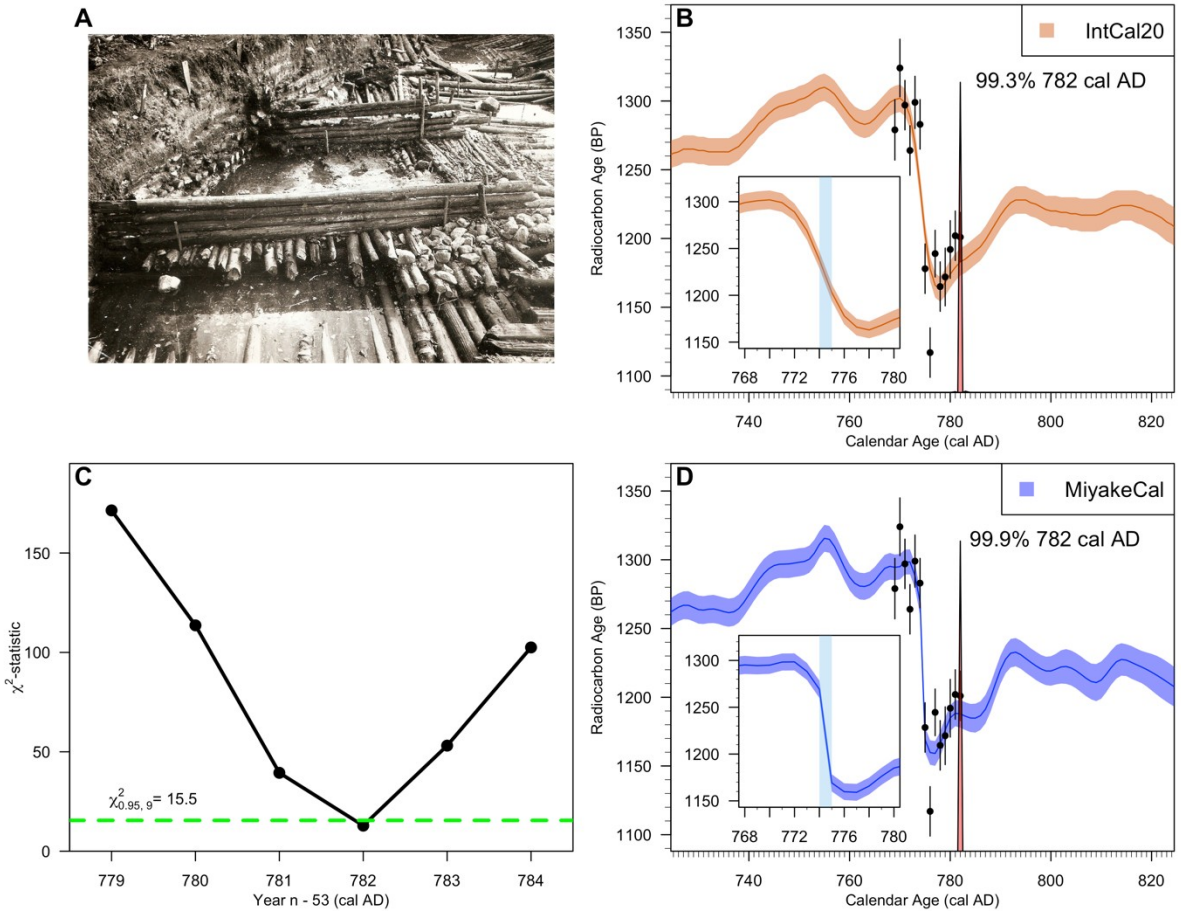

Figure I Panel A – Remains of Lake Āraiši timber fortress[60] (photograph by Jānis Apals). Panel B – Bayesian wiggle-match of 14 consecutive annual ^{14}C samples (black dots with 1σ error bars) against IntCal20 (orange with 1σ-intervals). The posterior calendar age estimate for the youngest ring in the sequence (n-53) is shown in red along the x-axis. Panel C – χ^2 wiggle-match testing of 9 Āraiši tree-rings against the mean of a set of NH tree-rings[54]. The only calendar year not rejected at the 5% level is cal AD 782. Panel D – Bayesian wiggle-match of 14 consecutive annual ^{14}C samples (black dots) against MiyakeCal (blue). Panel B and D insets show period of the increase in Δ^{14}C (decline in radiocarbon age) over the AD 774 event. The blue-shaded intervals show the year AD 774 in which the ESPE occurred. For an animation of Bayesian wiggle-matching, see SI video 2.

A frequently-used approach to obtaining exact calibration over an ESPE is wiggle-matching using a series of χ^2 tests which assess the fit of the ^{14}C sequence against the mean of known-age reference tree-ring datasets. Using the χ^2 approach, a series of independent hypothesis tests is performed, with each test shifting the ^{14}C sequence by a single calendar year and

assessing the fit to the reference. The resultant, e.g., 95% confidence interval for the calibrated age of the sequence consists of all calendar age fits which are not rejected at the 5 % significance level.

With χ^2 tests, users are restricted to considering only those growth-rings that overlap with the reference datasets for their chosen calendar fit. If the ^{14}C sequence to be wiggle-matched is longer than the reference[60,62], a χ^2 approach will therefore result in the loss of valuable calendar age information. For the Lake Āraiši fortress, to test each of six possible calendar fits (Figure I-C) against the standard reference[54] we are restricted to using only 9 of the 14 annual ^{14}C determinations. This provides a 95% confidence interval for ring *n-53* consisting of the single year cal AD 782. Users should also be aware that the current reference mean[54] does not incorporate the possibility of over-dispersion in the ^{14}C measurements, and it is possible no calendar age fits will pass the test.

Outside of ESPE calibration, Bayesian wiggle-matching against the suitable IntCal curve[6] is the standard method to calibrate ^{14}C sequences. This allows wiggle-matching of ^{14}C sequences of any length (although does not provide a measure of the overall quality-of-fit). The IntCal20 curve has not been popular for ESPE calibration since, due to its construction, sharp increases in $\Delta^{14}C$ are somewhat smoothed with the increase in $\Delta^{14}C$ over the AD 774 event occurring over the course of 4 calendar years (Figure I-B, inset). It is however still possible to obtain exact calibration using IntCal20 if the ^{14}C sequence to be calibrated is sufficiently long (Figure I-B). Using all 14 annual ^{14}C measurements from Lake Āraiši, we obtain a 99.3% probability that ring *n-53* is from cal AD 782.

Finally, if calibration curve construction is modified to permit an additional *non-smooth* jump in $\Delta^{14}C$ in the year AD 774–775, we can obtain a calibration curve that better represents the sharp ESPE signature. A Bayesian wiggle-match of the 14 annual measurements in the Āraiši ^{14}C sequence against the discontinuous *MiyakeCal* calibration curve suggests a 99.9% probability that ring *n-53* is from cal AD 782 (Figure I-D).

With all these alternative methods, our conclusions for Lake Āraiši are the same. With the waney-edge being 53 yrs after ring *n-53*, the fortress platform can be identified as having been built from trees felled between NH winter cal AD 835 and spring cal AD 836.

Case Study II

Regional timing of the AD 993 signature and implications for exact dating

The AD 993 ESPE is recorded by a sharp increase in $\Delta^{14}C$ in tree-rings globally. However, the precise timing of this increase is less clear (Figure II-A). Current data from a high-latitude region in Sweden[54] (NH0 >60º N) suggest that the major increase occurs between AD 992–993. Alternatively, trees collected from Mongolia and Russia[54] (NH1 40–60º N) suggest a two-year increase from AD 992–994. Finally, data from mid-latitude regions: two locations in China and USA[54] (NH2 30–40º N), and Japan[46,80] suggest the $\Delta^{14}C$ increase may occur between AD 993–994. The cause of these differences in phasing between tree-ring records is currently unknown. It has been suggested that the region (and specifically the latitude) in which the trees grew may be a key factor.

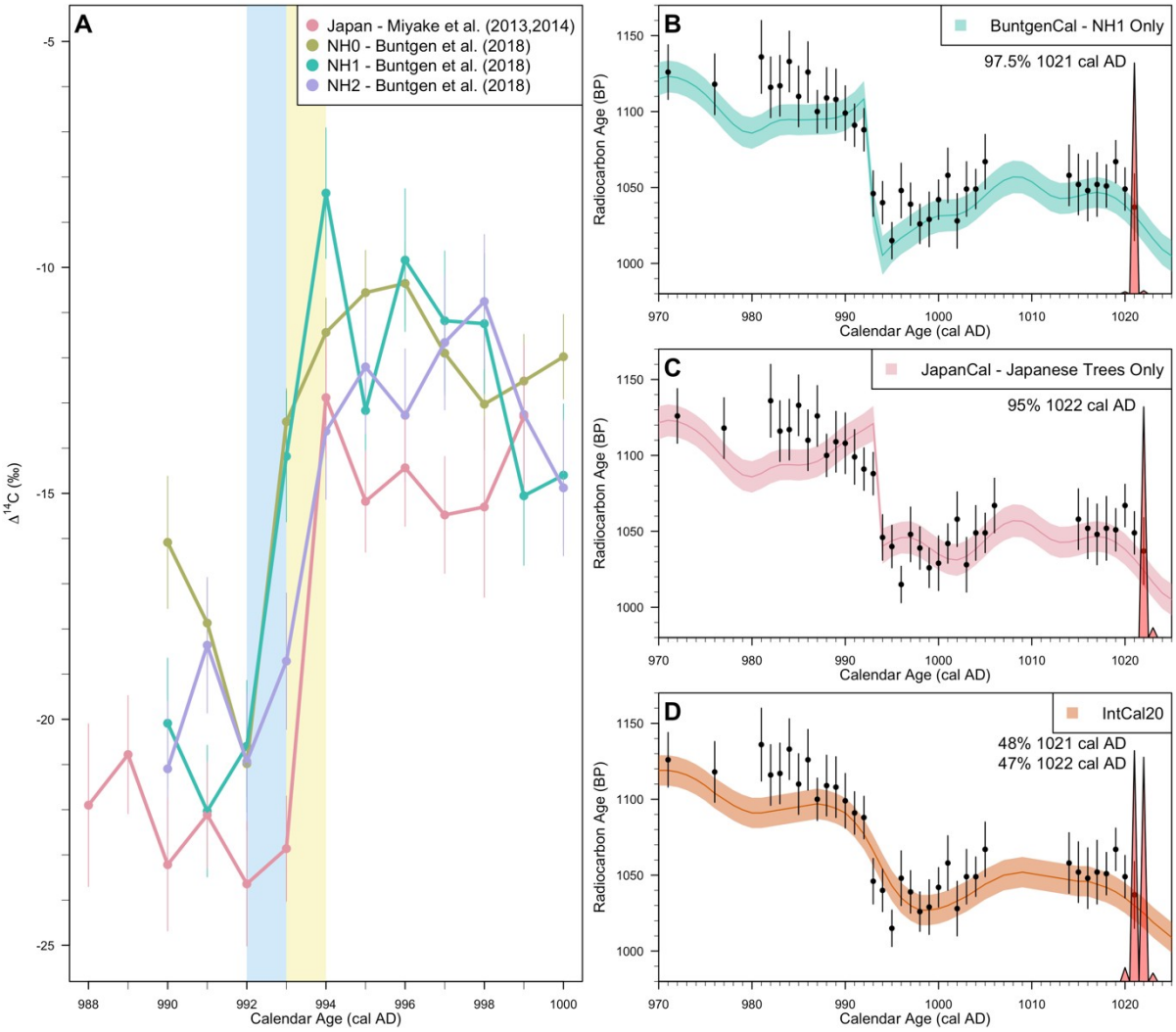

Figure II Difference in precise timing of the AD 993 ESPE in different NH tree-rings and the impact upon calibration over the event. Panel A: Weighted-average of observed $\Delta^{14}C$ (and 1σ error-bars) for the tree-rings in each NH zone[54] and the separate Japanese tree-rings[46,80]. Solid lines join the $\Delta^{14}C$ averages to illustrate when the $\Delta^{14}C$ increase occurs in each region. The shaded backgrounds correspond to AD 992–993 (light blue) and AD 993–994 (light yellow). Trees from different locations appear to record the ESPE spike in different years. Panel B: Calibration of wooden item 4A 68 E2-2 from L'Anse aux Meadows[62] (located at

51ºN) using the ^{14}C ages of all 35 annually-sampled growth rings (black dots with 1σ error-bars, covering 51 calendar years) against a preliminary calibration curve (shown in bluish-green with 1σ-intervals) created using only the NH1 ^{14}C datasets[54] in the region of the ESPE. Panel C: Calibration of the same item against a Japanese-based calibration curve (pink) created using only Japanese ^{14}C data[46,80]. Panel D: Calibration against the IntCal20 calibration curve[6] (orange) created using all the ^{14}C data in the Northern Hemisphere (from all NH zones[54] and the separate Japanese data[46,80]).

The choice of which ^{14}C reference data set to use to obtain exact ^{14}C calibration is crucial. In the case of wooden item 4A 68 E2-2[62] from L'Anse aux Meadows (at 51ºN), if we calibrate using the tree-rings from either NH0 or NH1[54] as the reference, we obtain a ca. 97% posterior probability that the waney edge is from cal AD 1021. Figure II-B presents wiggle-matching all 35 sampled annual growth rings of the item (covering 51 calendar years in total) against a calibration curve based upon only NH1 ^{14}C data[54]. Conversely if we calibrate against the reference Japanese tree-ring ^{14}C data[46,80] we obtain a ca. 95% probability that the waney edge is from cal AD 1022 (Figure II-C). Similar differences in calibrated ages are found for the other L'Anse aux Meadows items.

At present, the geographic coverage of reference ^{14}C data over the AD 993 event is somewhat limited[54]. More research, with sampling of ^{14}C data with a greater geographical spread and improved modelling of ^{14}C production and transport, is essential to understand the reasons behind the potential regional differences in the timing of the AD 993 ESPE signature. This will allow detailed guidance to be given to those seeking to use this event for exact calibration. When it is not known in which precise calendar year the ESPE will be recorded in sampled wood, to avoid potentially spurious precision it may be safer to calibrate against the IntCal20 curve which combines all the NH zonal and Japanese reference data (Figure II-D). This provides a ca. 48% posterior probability that the waney edge is from cal AD 1021, and a 47% probability it is from cal AD 1022.

Case Study III

Exploiting fine-scale structure in radiocarbon calibration: Wiggle-matching people

Background: In 2013, the remains of 28 men were excavated from Palace Green, Durham, UK[74,75]. Samples from four skeletons were dated, all of which were recovered from two mass graves thought to have been made at the same time. One grave was stratified below the Bishop's Stables, which is shown on a map of AD 1754, and, as the dentition of two individuals shows pipe-facets (Figure III-B), the mass burial must have occurred after c. AD 1620 when tobacco from the Virginia plantations made clay pipes widely available across Britain[81].

Question: Could these graves be prisoners from the Battle of Dunbar (3 September AD 1650)?

Relative Dating Information: For skeletons Sk12 and Sk21, it was possible to obtain ^{14}C samples formed at different times of development. This allows relative dating to be incorporated into calibration. The upper half of the root of the first molar, which forms at 4–6 years of age, and the upper half of the root of the third molar, which forms at 14–16 years of age[82] were sampled from Sk12 and Sk21. As these individuals died aged 19–23 years and 21–25 years respectively, the calendar gap between the teeth can be incorporated in the model as 10±1 years, followed by the gap to the individuals' deaths as 6±1 years and 8±1 years respectively. For Sk9, an individual who died aged 17, and Sk16A, an individual who died aged 14, an allowance has been made for the turnover time of the sampled bones (a femur and a tibia respectively)[70], equating to 5±2 years and 4±2 years respectively. Combining the two molars for Sk12 and Sk21 with the two bones for Sk9 and Sk16A, and assuming a common date of death, provides a sequence of six ^{14}C determinations to be wiggle-matched using variable gaps between each sample.

Dietary Information: The proportion of marine foods in each individual's diet was estimated from the ratio of stable carbon isotopes in the skeleton, and a bespoke calibration curve for each individual constructed incorporating this[83]. The marine component is modelled using the Marine20 calibration curve[7] with a local ΔR_{20} value of −133±33 BP calculated from the 10 closest points to Durham in the Marine20 reservoir database (http://calib.org/marine/, accessed 27 April 2023)[84]. The remaining proportion of the diet was modelled using the terrestrial IntCal20 calibration curve[6].

Calibrating a single sample: A simple analysis of the graves might

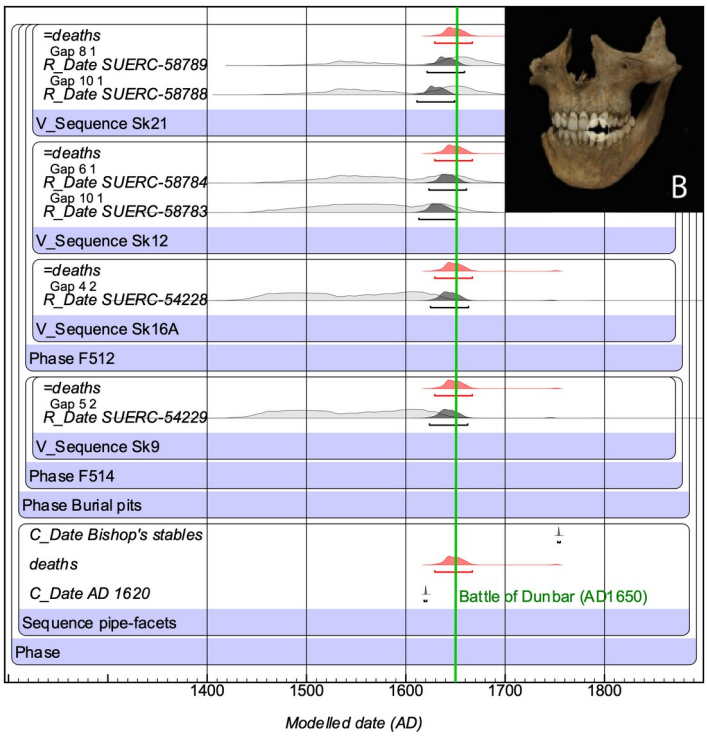

Figure III Panel A: Part of chronological model IID[74] for mass graves excavated on the Palace Green, Durham, UK (run in OxCal[13]). Panel B: Skull of skeleton 21, showing pipe-facets (highlighted) caused by the habitual use of a tobacco pipe.

just consider calibration of Sk12's third molar (SUERC-58784). Calibration of this single ^{14}C measurement provides a date of death for Sk12 spanning cal AD 1480–1696, 1742–1761 and 1768–1806 (HPD interval at 95% probability, see grey shaded distribution in Figure III-A). This calibrated age range is potentially compatible with the Battle of Dunbar, but its wide breadth weakens any inference on the specific circumstances of death.

Chronological modelling incorporating archaeological information: Jointly calibrating all the skeletons within the grave and incorporating the available stratigraphic, historical, and biological information enables a substantial increase in calendar age precision. The resultant model (Figure III-A) estimates that the individuals buried in the mass graves died in cal AD 1630–1670 (HPD interval at 95% probability). A much narrower calendar range than achievable via calibration of just a single sample and clearly compatible with the Battle of Dunbar.

Future Directions and Opportunities

Understanding the Sun

For the period before telescopes (pre-early 17th century), cosmogenic isotopes provide the only quantitative information on solar variability – in particular ^{14}C due to its high resolution. Models that link cosmogenic production and solar variability can be verified using direct instrumental data on the Sun obtained over the last four centuries[41,85,86].

All eight Holocene ESPEs identified so far were 20–100 times stronger than the strongest solar storm directly recorded over the past decades (on 23rd February AD 1956). The 12,350 BC event still needs detailed analysis but has the largest $\Delta^{14}C$ increase of all[45]. However, smaller ESPEs cannot be resolved in the existing ^{14}C data series[30,31]. Presently, only ~1/6 of the Holocene is covered with high-resolution ^{14}C data[6,42]. It is therefore likely that more ESPEs will be found as the coverage of precise annual ^{14}C measurements increases.

Increasing annual coverage is crucial to fully understand ESPEs. It is still unclear whether they correspond to the very energetic tail of rare but 'regular' solar storms, so-called *Black Swan* events[87]; or represent an entirely new solar eruptive process, *Dragon King* events (Figure 3). In 2012, super-flares on sunlike stars that are 100–1000 times stronger than all known solar flares were also discovered[88]. It has been proposed that ESPEs and super-flares are related phenomena. However, a projection of super-flare results to the Sun does not match the ESPE statistics[89]. To resolve these questions, more high-precision ^{14}C measurements, reproduced over multiple records at annual resolution, are needed.

Solar activity is organized in ~11-year cycles of slightly variable lengths and strongly variable amplitude[90]. These cycles are traditionally studied by sunspot numbers. Observations of sunspot numbers began in AD 1610 and form the longest dataset of direct astronomical observations, covering 36 solar cycles including the Maunder minimum of activity (AD 1645–1715) and a Modern grand maximum (AD 1940–2008). This time series allows some empirical regularities of the solar cycle to be identified[90] but is highly limited as the number of cycles is small.

Annual ^{14}C data has been used to study solar cycles beyond the observational sunspot record for some time[19] but was previously hampered by insufficient measurement resolution. In 2021, ^{14}C measurements for the last millennium were obtained with precision sufficient to reconstruct individual solar cycles[41,85]. This has nearly tripled the number of known solar cycles to 96 and allowed some empirical rules to be confirmed. Further reconstruction of 11-year solar cycles on longer multi-millennial time scale, something only possible with high-precision annual ^{14}C measurements, is critical to understanding the solar dynamo[91].

So far, excluding the 12,350 BC event[45], ESPEs have only been found in Holocene subfossil trees. Solar variability beyond the Holocene remains *terra incognita* although existing tree-ring ^{14}C data and ice core ^{10}Be and ^{36}Cl are seen to exhibit high-frequency structures[50,92–94]. Extending the solar record beyond the Holocene will require dedicated efforts to find relatively rare subfossil trees from the Glacial and Late Glacial periods. Ancient New Zealand kauri (*Agathis australis*) shows considerable promise beyond the last glacial

maximum[50,51]. The AMS analyses of these trees will need to be optimized through careful controls on uncertainty[95] to detect small and rapid ^{14}C changes. The Glacial and Late Glacial periods were characterized by rapid variations of the carbon cycle as illustrated by changes of atmospheric $^{12}CO_2$[96] and $^{13}CO_2$[97]. This emphasizes the need to reconstruct abrupt ^{14}C changes in trees from both hemispheres. Abrupt solar variations should be recorded in all trees whereas rapid carbon cycle changes may lead to changes in the interhemispheric ^{14}C gradient[98,99].

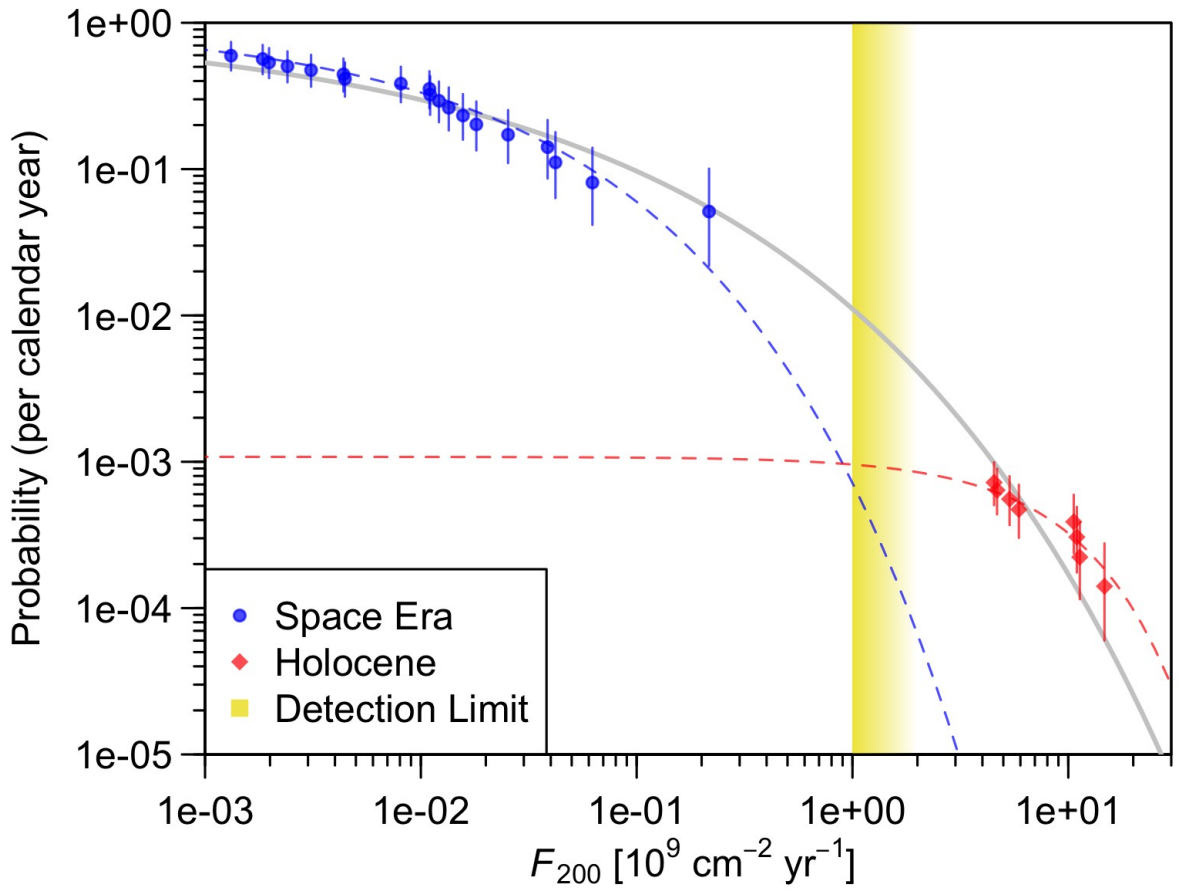

Figure 3 Estimated probabilities that, in any given year, the annual F_{200} fluence will exceed specific values, as assessed from direct data for the space era (blue circles)[100] *and cosmogenic isotope data for the Holocene (red diamonds). Data shown with 90% confidence intervals. The vertical yellow bar indicates the current sensitivity/detection limit of the cosmogenic-isotope method for a single ^{14}C record*[31]*, with ESPEs lying to the right. The current lack of information near this limit prevents us from distinguishing between the Black-Swan scenario where ESPEs are the tail of regular solar storms and all data can be fitted with a single distribution (Weibull – grey curve); and the Dragon-King scenario where ESPEs and regular storms are distinct physical phenomena following separate distributions (dashed red and blue curves respectively)*[87]*. Further high-precision annual ^{14}C*

measurements, reproduced over multiple records, will lower the detection limit and resolve this.

Understanding Environmental Processes

Abrupt spikes in ^{14}C production enable insight into Earth and environmental processes. Sub-annual ^{14}C measurements across the AD 774 and AD 993 Miyake events from the mid- to high-latitudes of both hemispheres have helped identify the seasonal timing and a latitudinal gradient of radiocarbon preserved in contemporary trees[54]. Intriguingly, these early results suggest there may be regional differences in the precise timings of some ESPE ^{14}C signatures (Case Study II) and in the interhemispheric ^{14}C gradient between the events, possibly modulated by changes in the ocean-atmospheric circulation and the carbon cycle[54].

To improve our understanding of Earth system processes, high-precision annual (or even sub-annual) ^{14}C measurements must be accompanied by development of a carbon-cycle dynamical model with sufficient spatio-temporal accuracy to account for detailed processes including latitudinal gradients, orography, proximity to the ocean, and the growth period of trees. While the standard carbon-cycle box model[101] works well for slow decadal changes, large-scale 'boxes' that do not resolve uneven patterns of ^{14}C production and transport may lead to inaccurate results for (sub-)annual scales, especially during ESPE production spikes[102]. A prospective direction is coupling a detailed climate-chemistry dynamical atmospheric model (e.g., SOCOL[103], ECHAM-HAM or GEOS-Chem[104]) with the dynamical ocean[105] and a realistic biosphere, including growth and carbon uptakes of specific tree species.

With the carbon cycle currently experiencing extreme disruption[106], the scientific community is using inverse 3D-transport modelling to identify CO_2 emission sources and sinks based on the time-varying spatial evolution of $^{12}CO_2$, $^{13}CO_2$ and $^{14}CO_2$[107–109]. Application of this approach using ^{14}C records of ESPE spikes and other rapid ^{14}C changes at different locations may improve knowledge on natural ^{14}C atmospheric dispersal and carbon sinks, extending the insights afforded by the 1960s nuclear 'bomb spike'[110]. Complemented by an expanded global network of ^{14}C measurements, such an approach would allow use of the observed latitudinal gradients in the amplitude of ESPEs[54]. Similar chemical transport models could be used to simulate the dispersal and fallout of ^{10}Be and ^{36}Cl on polar ice caps[104,111]. This is crucial since aerosols from volcanic eruptions can enhance ^{10}Be and ^{36}Cl deposition, generating abrupt spikes which may be confused with ESPEs[112]. Accurate geomagnetic records[113] are also necessary to model the amplitude of cosmogenic production associated with ESPEs.

606 ***Statistical Considerations***

607 Harnessing annual-resolution calibration datasets will require statistical hurdles to be
608 overcome. Calibration curve construction must be adapted to better represent abrupt ESPE
609 ^{14}C production changes. This is a challenge, as regression methods typically assume that the
610 underlying function is smooth[114] to prevent overfitting. Ensuring one does not overfit to
611 spurious ^{14}C artefacts is particularly important for calibration curves since the underlying
612 reference data consist of overlapping trees from different locations, species, and laboratories
613 all of which introduce considerable additional variability[115–117].

614 Such smoothness does not however easily permit representation of ESPEs. One solution
615 might incorporate additional *ESPE-specific* basis functions, placed at fixed times, into the
616 regression to represent the temporal atmospheric $\Delta^{14}C$ response of an ESPE. These functions
617 could be informed by the atmospheric models discussed above[103,104]. This will require
618 agreement on where such additional basis functions should be located and, until coverage
619 with annual ^{14}C data becomes complete, leaves the possibility that some ESPE variations will
620 be missed in the calibration curves[42].

621 With increasing calibration precision, it is essential to fully understand all sources of potential
622 variations in the measurement of ^{14}C samples including shared offsets and biases[115]. This is
623 particularly relevant for annual measurements due to ^{14}C differences during the growing
624 season[54,117,118]. Current tree-ring data exhibit over-dispersion with ^{14}C measurements in any
625 calendar year more highly spread than their quoted laboratory-reported uncertainties should
626 suggest[53]. Furthermore, consistent ^{14}C offsets have been observed between contemporaneous
627 tree rings from different locations (e.g., Case Study II where, in addition to a difference in
628 ESPE timing, the ^{14}C measurements from any region tend to stay above/below those of other
629 regions). Understanding the causes for additional variations and shared biases in ^{14}C is critical
630 to accurate calibration, particularly when calibrating sequences of ^{14}C samples (Case Study II
631 and Figure 4).

632 The ^{14}C community has undertaken considerable work to assess and improve the accuracy
633 and precision of their measurements via laboratory intercomparisons[95,119]. This work has
634 begun to apportion the sources of variation observed in ^{14}C measurements (e.g., pre-treatment
635 methods). Identification of offsets and their sources is however challenging since they are
636 typically of a similar size to measurement precision. Furthermore, many offsets will not be
637 constant over time[115]. We require a dedicated programme of work, engaging with a broad set
638 of laboratories, to improve our understanding of regional, altitudinal, and laboratory sources
639 of additional uncertainty, aided by high-precision AMS.

640 Calibration curve usage could potentially be improved by use of covariance information on
641 the ^{14}C ages in adjacent calendar years. This is currently lost when providing pointwise curve
642 summaries[53,120]. Additionally, as calibration curves becomes wigglier, the possibility of highly
643 multimodal fits when calibrating models increases substantially. Use of robust assessment
644 metrics[13,121–124] to ensure calibration models have properly converged before inference is made
645 will be even more essential than at present. More advanced Markov Chain Monte Carlo
646 approaches such as parallel tempering[53,125], slice sampling[126,127], or Hamiltonian Monte
647 Carlo[128] may become required.

To ensure uptake amongst the radiocarbon community, all these statistical considerations must be integrated into user-friendly software, accompanied by educational support.

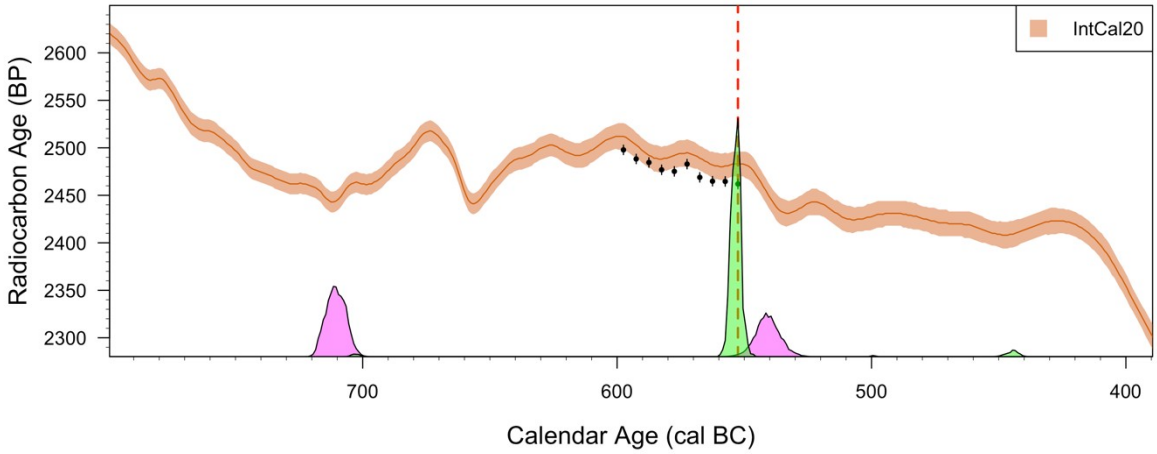

Figure 4: Implications of a ^{14}C offset when wiggle-matching over a plateau. A sequence of 10 ^{14}C samples (black dots with 1σ error-bars) beginning in 552 BC has been simulated which share an offset/bias of 16 ^{14}C yr from the IntCal20 curve (orange curve with 1σ-intervals). The vertical red line represents the true underlying calendar age. If we take the default approach to wiggle-matching, assuming measurement error is independent, the posterior age density (magenta) is bimodal and inaccurate. However, if we perform a wiggle-match incorporating the possibility of an offset shared by all 10 ^{14}C measurements, the sequence calibrates accurately and precisely (green posterior age density).

Archaeological Interpretations

Since ^{14}C dating was first developed, archaeological adoption of new developments has been rapid. The possibility of obtaining exact chronologies by fitting series of measurements on single-year tree-rings to the abrupt changes in atmospheric ^{14}C at ESPEs is the latest example[56–62]. This methodology can provide precise calendar dating for particular sites that fits them exactly into historical narratives, thus providing fixed points within wider archaeological discussion. It also has the potential to securely anchor floating historical sequences, such as those of the Near East and Central America, to the calendar scale[129]. The search for key timbers, intact to waney edge and securely tied to these historical sequences, marches in parallel with the hunt for new ESPEs.

For archaeologists studying sites or periods containing known ESPEs, dating a series of single tree-rings containing the specific ESPE signature may provide an exact anchoring for that chronology. The relationship between the dated sample and the archaeological question, however, remains paramount[14,130]. For long periods, however, there are no such events. As more single-year data become available, changes to the calibration curve in some periods will be substantial, particularly if there is a currently undetected ESPE[42]. In most places however, changes will be more modest with small wiggles and steps becoming visible which cannot be resolved in the current coarser-resolution data[95]. This additional structure, even on a small scale, can nevertheless still have a substantive impact on modelled chronologies.

Archaeologists have long focused on the inbuilt age and taphonomy of the material selected for dating[131] and, with the advent of AMS, came a focus on dating short-life, single-entity samples[132]. The current Bayesian process[14] provides a framework to select suites of samples for dating that can be interpreted together in formal statistical models. This process will need to develop in the face of a much more detailed annual calibration curve, in particular the possibility to leverage information from short ^{14}C sequences and/or sequences of short-lived ^{14}C samples more effectively (Case Study III). In undertaking such studies, high-precision measurement of the unknown samples is vital[133]. Increases in the modelling of suites of ^{14}C samples may be supported by development of model selection approaches, building upon existing individual and model agreement indices[124]. Such approaches could provide more robust inference in the presence of model uncertainty[134,135] and help select between multiple potential interpretations.

Finally, the increase in the detail and precision of calibration data mean it is essential to ensure reproducibility of ^{14}C modelling. Each update to the calibration datasets affects the calibrated dates in previous studies. There is a need to develop model repositories where, as calibration curves are improved, previous studies can be recalibrated with the state-of-the-art knowledge. This will ensure research remains comparable, and archaeological/geoscientific knowledge is continuously updated.

Conclusions

The unexpected discovery of extreme solar particle events in the ^{14}C record has brought together archaeologists, environmental scientists, and solar physicists in pursuit of common research objectives. ESPEs, and the extensive high-precision annual ^{14}C measurement programmes their discovery initiated, are enabling substantial advances across numerous fields of endeavour. In addition to improvements in the dating precision achievable using radiocarbon, including the potential calibration to an exact year, we are now gaining deep insights into our Sun's extreme behaviour, societal evolution and the archaeological record, and the operation of the Earth system. Whether used for precise dating, or solar physics, radiocarbon has shown itself to remain fundamental to understanding the world in which we live.

Supplementary Information (Videos/Animations and Legend)

SI Video 1: Animation of calibrating the 3350 ± 10 BP[9,11] Thera ^{14}C date of Fig. 1. For each calendar year, the corresponding ^{14}C age of the IntCal20 calibration curve is shown with black dashed lines. Black dots and lines follow the heights of the probability distributions of the radiocarbon date (dark magenta) and the calibrated age (light magenta). Note that while the dashed lines only connect to the mean calibration curve (orange line), the calibrated distribution combines the uncertainties of both the ^{14}C date and the calibration curve (orange envelope).

SI Video 2: Animation of wiggle-match dating of the Lake Āraiši ^{14}C sequence (black dots and 1σ error bars) against the MiyakeCal curve (blue; see Fig. 2B). For each calendar year, the corresponding ^{14}C age of the IntCal20 calibration curve is shown with dark green dashed lines. Dark green dots and lines follow the heights of the probability distributions of the radiocarbon and calibrated dates (light green). Wiggle-match distribution using the spacing between the dated tree-rings is shown in magenta. The calibrated and wiggle-matched distributions combine the uncertainties of both the ^{14}C dates and the calibration curve.

End Notes

Acknowledgments: We thank Z Apala and J Apals for the photograph in Case Study I, and J Veitch for the Sk21 photograph (© Department of Archaeology, Durham University) in Case Study III. We also acknowledge K Hemer, J Meadows, A Millard, EM Scott, and G Stone for their feedback. IU benefitted from the visiting fellowship programme at ISSI (Bern).

Funding: TJH was supported by APX\R1\231120, NE/X009815/1, and EP/X032906/1. EB is funded by ANR MARCARA. CBR is supported by NE/X009815/1 and as part of the National Environmental Isotope Facility (NEIF). IU acknowledges partial support from the Research Council of Finland (project 354280).

Author Contributions: All authors contributed to the development of ideas for the perspective, the writing of initial drafts, and subsequent revisions.

Competing interests: The authors declare no competing interests.

Data Availability: All data is available in accompanying references.

Code Availability: Code is available at https://github.com/TJHeaton/Quest-Exact-Radiocarbon-Dating

Additional Information: Supplementary Information is available for this paper. Correspondence and requests for materials should be addressed to TJ Heaton (t.heaton@leeds.ac.uk).

References

1. Ruben, S. & Kamen, M. D. Radioactive Carbon of Long Half-Life. *Phys. Rev.* **57**, 549 (1940).

2. Taylor, R. E. & Bar-Yosef, O. *Radiocarbon Dating: An Archaeological Perspective*. (Routledge, 2014). doi:https://doi.org/10.4324/9781315421216.

3. Heaton, T. J. *et al.* Radiocarbon: A key tracer for studying Earth's dynamo, climate system, carbon cycle, and Sun. *Science* **374**, eabd7096 (2021).

4. Arnold, J. R. & Libby, W. F. Age Determinations by Radiocarbon Content: Checks with Samples of Known Age. *Science* **110**, 678–680 (1949).

5. Libby, W. F., Anderson, E. C. & Arnold, J. R. Age Determination by Radiocarbon Content: World-Wide Assay of Natural Radiocarbon. *Science* **109**, 227–228 (1949).

6. Reimer, P. J. *et al.* The IntCal20 Northern Hemisphere Radiocarbon Age Calibration Curve (0–55 cal kBP). *Radiocarbon* **62**, 725–757 (2020).

7. Heaton, T. J. *et al.* Marine20—The Marine Radiocarbon Age Calibration Curve (0–55,000 cal BP). *Radiocarbon* **62**, 779–820 (2020).

8. Hogg, A. G. *et al.* SHCal20 Southern Hemisphere Calibration, 0–55,000 Years cal BP. *Radiocarbon* **62**, 759–778 (2020).

9. Bronk Ramsey, C., Manning, S. W. & Galimberti, M. Dating the Volcanic Eruption at Thera. *Radiocarbon* **46**, 325–344 (2004).

10. Pearson, C., Sbonias, K., Tzachili, I. & Heaton, T. J. Olive shrub buried on Therasia supports a mid-16th century BCE date for the Thera eruption. *Sci Rep* **13**, 6994 (2023).

11. Bruins, H. J. *et al.* Geoarchaeological tsunami deposits at Palaikastro (Crete) and the Late Minoan IA eruption of Santorini. *J Archaeol Sci* **35**, 191–212 (2008).

12. Buck, C. E., Cavanagh, W. G. & Litton, C. D. *Bayesian Approach to Interpreting Archaeological Data*. (John Wiley & Sons Ltd, Chichester, 1996).

13. Bronk Ramsey, C. Bayesian Analysis of Radiocarbon Dates. *Radiocarbon* **51**, 337–360 (2009).

14. Bayliss, A. & Marshall, P. *Radiocarbon Dating and Chronological Modelling: Guidelines and Best Practice*. (Historic England, London, 2022).

15. Bronk Ramsey, C. *et al.* Improved age estimates for key Late Quaternary European tephra horizons in the RESET lattice. *Quat Sci Rev* **118**, 18–32 (2015).

16. Bayliss, A. *et al.* Informing Conservation: Towards ^{14}C Wiggle-Matching of Short Tree-Ring Sequences from Medieval Buildings in England. *Radiocarbon* **59**, 985–1007 (2017).

17. Bard, E., Raisbeck, G. M., Yiou, F. & Jouzel, J. Solar modulation of cosmogenic nuclide production over the last millennium: comparison between ^{14}C and ^{10}Be records. *Earth Planet Sci Lett* **150**, 453–462 (1997).

Muscheler, R. *et al.* Solar activity during the last 1000yr inferred from radionuclide records. *Quat Sci Rev* **26**, 82–97 (2007).

Stuiver, M. & Braziunas, T. F. Sun, ocean, climate and atmospheric $^{14}CO_2$: an evaluation of causal and spectral relationships. *Holocene* **3**, 289–305 (1993).

Miyake, F., Nagaya, K., Masuda, K. & Nakamura, T. A signature of cosmic-ray increase in AD 774–775 from tree rings in Japan. *Nature* **486**, 240–242 (2012).

Discovery of first (AD 774) Miyake event initially assumed to be due to a supernova.

Mekhaldi, F. *et al.* Multiradionuclide evidence for the solar origin of the cosmic-ray events of AD 774/5 and 993/4. *Nat Commun* **6**, 8611 (2015).

Usoskin, I. G. *et al.* The AD775 cosmic event revisited: the Sun is to blame. *A&A* **552**, L3 (2013).

Proof of solar origin of the AD 774 Miyake event and introduction of ESPE term.

Ritter, S. *et al.* International Legal and Ethical Issues of a Future Carrington Event: Existing Frameworks, Shortcomings, and Recommendations. *New Space* **8**, 23–30 (2020).

Oughton, E. J., Skelton, A., Horne, R. B., Thomson, A. W. P. & Gaunt, C. T. Quantifying the daily economic impact of extreme space weather due to failure in electricity transmission infrastructure. *Space Weather* **15**, 65–83 (2017).

Atwater, B. F. Evidence for Great Holocene Earthquakes Along the Outer Coast of Washington State. *Science* **236**, 942–944 (1987).

Winkler, T. S. *et al.* Revising evidence of hurricane strikes on Abaco Island (The Bahamas) over the last 700 years. *Sci Rep* **10**, 16556 (2020).

Wilhelm, B. *et al.* Impact of warmer climate periods on flood hazard in the European Alps. *Nat Geosci* **15**, 118–123 (2022).

Mook, W. G. Business Meeting: Recommendations/Resolutions Adopted by the Twelfth International Radiocarbon Conference. *Radiocarbon* **28**, 799 (1986).

Stuiver, M. & Polach, H. A. Discussion Reporting of ^{14}C Data. *Radiocarbon* **19**, 355–363 (1977).

Mekhaldi, F., Adolphi, F., Herbst, K. & Muscheler, R. The Signal of Solar Storms Embedded in Cosmogenic Radionuclides: Detectability and Uncertainties. *J Geophys Res Space Phys* **126**, e2021JA029351 (2021).

Usoskin, I. G. *et al.* Revisited Reference Solar Proton Event of 23 February 1956: Assessment of the Cosmogenic-Isotope Method Sensitivity to Extreme Solar Events. *J Geophys Res Space Phys* **125**, e2020JA027921 (2020).

Sukhodolov, T. *et al.* Atmospheric impacts of the strongest known solar particle storm of 775 AD. *Sci Rep* **7**, 45257 (2017).

Koldobskiy, S., Mekhaldi, F., Kovaltsov, G. & Usoskin, I. Multiproxy Reconstructions of Integral Energy Spectra for Extreme Solar Particle Events of

7176 BCE, 660 BCE, 775 CE, and 994 CE. *J Geophys Res Space Phys* **128**, e2022JA031186 (2023).

Clette, F. *et al.* Recalibration of the Sunspot-Number: Status Report. *Sol Phys* **298**, 44 (2023).

Hudson, H. S. Carrington Events. *Annu Rev Astron Astrophys* **59**, 445–477 (2021).

Uusitalo, J. *et al.* Transient Offset in ^{14}C After the Carrington Event Recorded by Polar Tree Rings. *Geophys Res Lett* **51**, e2023GL106632 (2024).

Suter, M., Huber, R., Jacob, S. A. W., Synal, H.-A. & Schroeder, J. B. A new small accelerator for radiocarbon dating. *AIP Conf Proc* **475**, 665–667 (1999).

Synal, H.-A., Stocker, M. & Suter, M. MICADAS: A new compact radiocarbon AMS system. *Nucl Instrum Methods Phys Res B* **259**, 7–13 (2007).

Synal, H.-A. & Wacker, L. AMS measurement technique after 30years: Possibilities and limitations of low energy systems. *Nucl Instrum Methods Phys Res B* **268**, 701–707 (2010).

O'Hare, P. *et al.* Multiradionuclide evidence for an extreme solar proton event around 2,610 B.P. (~660 BC). *Proceedings of the National Academy of Sciences* **116**, 5961–5966 (2019).

Discovery of confirmed 660 BC ESPE with multi-proxy analysis.

Brehm, N. *et al.* Eleven-year solar cycles over the last millennium revealed by radiocarbon in tree rings. *Nat Geosci* **14**, 10–15 (2021).

Brehm, N. *et al.* Tree-rings reveal two strong solar proton events in 7176 and 5259 BCE. *Nat Commun* **13**, 1196 (2022).

Discovery of confirmed 7176 BC and 5259 BC ESPEs.

Paleari, C. I. *et al.* Cosmogenic radionuclides reveal an extreme solar particle storm near a solar minimum 9125 years BP. *Nat Commun* **13**, 214 (2022).

Miyake, F. *et al.* A Single-Year Cosmic Ray Event at 5410 BCE Registered in ^{14}C of Tree Rings. *Geophys Res Lett* **48**, e2021GL093419 (2021).

Bard, E. *et al.* A radiocarbon spike at 14,300 cal yr BP in subfossil trees provides the impulse response function of the global carbon cycle during the Late Glacial. *Philosophical Transactions of the Royal Society A* **381**, 20220206 (2023).

Largest annual increase in $\Delta^{14}C$, and only pre-Holocene event, discovered so far.

Miyake, F., Masuda, K. & Nakamura, T. Another rapid event in the carbon-14 content of tree rings. *Nat Commun* **4**, 1748 (2013).

Discovery of second (AD 993) Miyake event showing the events recur.

Stuiver, M. A Note on Single-Year Calibration of the Radiocarbon Time Scale, AD 1510–1954. *Radiocarbon* **35**, 67–72 (1993).

48. Southon, J., Noronha, A. L., Cheng, H., Edwards, R. L. & Wang, Y. A high-resolution record of atmospheric ^{14}C based on Hulu Cave speleothem H82. *Quat Sci Rev* **33**, 32–41 (2012).

49. Cheng, H. *et al.* Atmospheric $^{14}C/^{12}C$ changes during the last glacial period from Hulu Cave. *Science* **362**, 1293–1297 (2018).

50. Cooper, A. *et al.* A global environmental crisis 42,000 years ago. *Science* **371**, 811 – 818 (2021).

51. Hogg, A. G. *et al.* Advances and limitations in establishing a contiguous high-resolution atmospheric radiocarbon record derived from subfossil kauri tree rings for the interval 60–27 cal kyr BP. *Quat Geochronol* **68**, 101251 (2022).

52. Reimer, P. J. *et al.* Selection and treatment of data for radiocarbon calibration: An update to the international calibration (IntCal) criteria. *Radiocarbon* **55**, 1923–1945 (2013).

53. Heaton, T. J. *et al.* The IntCal20 Approach to Radiocarbon Calibration Curve Construction: A New Methodology Using Bayesian Splines and Errors-in-Variables. *Radiocarbon* **62**, 821–863 (2020).

54. Büntgen, U. *et al.* Tree rings reveal globally coherent signature of cosmogenic radiocarbon events in 774 and 993 CE. *Nat Commun* **9**, 3605 (2018).

Evidence of global ESPE signatures enabling use for annual-precision ^{14}C calibration.

55. Reimer, P. J. *et al.* IntCal13 and Marine13 radiocarbon age calibration curves 0-50,000 years cal BP. *Radiocarbon* **55**, 1869–1887 (2013).

56. Wacker, L. *et al.* Radiocarbon Dating to a Single Year by Means of Rapid Atmospheric ^{14}C Changes. *Radiocarbon* **56**, 573–579 (2014).

First usage of ESPEs to provide annual-precision dating using ^{14}C.

57. Hakozaki, M. *et al.* Verification of the Annual Dating of the 10th Century Baitoushan Volcano Eruption Based on an AD 774–775 Radiocarbon Spike. *Radiocarbon* **60**, 261–268 (2018).

58. Kuitems, M. *et al.* Radiocarbon-based approach capable of subannual precision resolves the origins of the site of Por-Bajin. *Proceedings of the National Academy of Sciences* **117**, 14038–14041 (2020).

59. Oppenheimer, C. *et al.* Multi-proxy dating the 'Millennium Eruption' of Changbaishan to late 946 CE. *Quat Sci Rev* **158**, 164–171 (2017).

60. Meadows, J., Zunde, M., Lēģere, L., Dee, M. W. & Hamann, C. Single-year ^{14}C dating of the lake-fortress at Āraiši, Latvia. *Radiocarbon* **(to appear)**, (2023).

61. Philippsen, B., Feveile, C., Olsen, J. & Sindbæk, S. M. Single-year radiocarbon dating anchors Viking Age trade cycles in time. *Nature* **601**, 392–396 (2022).

Annual dating for the start of the Viking Age using the AD 774 ESPE.

62. Kuitems, M. *et al.* Evidence for European presence in the Americas in AD 1021. *Nature* **601**, 388–391 (2022).

Dating of year that Vikings were present in N America using AD 993 ESPE.

Black, B. A. *et al.* A multifault earthquake threat for the Seattle metropolitan region revealed by mass tree mortality. *Sci Adv* **9**, eadh4973 (2023).

Maczkowski, A. *et al.* Absolutely dating the European Neolithic through a rapid ^{14}C excursion. *PREPRINT (Version 1) available at Research Square* (2023) doi:10.21203/rs.3.rs-3419721/v1.

Manning, S. W., Birch, J., Conger, M. A. & Sanft, S. Resolving Time among Non-Stratified Short-Duration Contexts on a Radiocarbon Plateau: Possibilities and Challenges from the AD 1480–1630 Example and Northeastern North America. *Radiocarbon* **62**, 1785–1807 (2020).

Nakao, N., Sakamoto, M. & Imamura, M. ^{14}C Dating of Historical Buildings in Japan. *Radiocarbon* **56**, 691–697 (2014).

Capano, M. *et al.* Is the dating of short tree-ring series still a challenge? New evidence from the pile dwelling of Lucone di Polpenazze (northern Italy). *J Archaeol Sci* **121**, 105190 (2020).

Djamali, M. *et al.* An absolute radiocarbon chronology for the world heritage site of Sarvestan (SW Iran): A late Sasanian heritage in early Islamic era. *Archaeometry* **64**, 545–559 (2022).

Jull, A. J. T., Burr, G. S. & Hodgins, G. W. L. Radiocarbon dating, reservoir effects, and calibration. *Quaternary International* **299**, 64–71 (2013).

Gosman, J. H., Hubbell, Z. R., Shaw, C. N. & Ryan, T. M. Development of Cortical Bone Geometry in the Human Femoral and Tibial Diaphysis. *Anat Rec* **296**, 774–787 (2013).

Ubelaker, D. H. *et al.* Lag time of modern bomb-pulse radiocarbon in human bone tissues: New data from Brazil. *Forensic Sci Int* **331**, 111143 (2022).

Rose, H. A., Meadows, J. & Bjerregaard, M. High-Resolution Dating of a Medieval Multiple Grave. *Radiocarbon* **60**, 1547–1559 (2018).

Chmielewski, T. J. *et al.* Increase in ^{14}C dating accuracy of prehistoric skeletal remains by optimised bone sampling: Chronometric studies on eneolithic burials from Mikulin 9 (Poland) and Urziceni-Vada Ret (Romania). *Geochronometria* **47**, 196–208 (2020).

Millard, A. *Palace Green Library Excavations 2013 (PGL13): Chronology of the Burials*. https://www.dur.ac.uk/resources/archaeology/pdfs/PGL13_Chronology_Report.pdf (2015).

Gerrard, C., Graves, P., Millard, A., Annis, R. & Caffell, A. *Lost Lives, New Voices: Unlocking the Stories of the Scottish Soldiers from the Battle of Dunbar, 1650*. (Oxbow, Oxford, 2018).

Douka, K. *et al.* Age estimates for hominin fossils and the onset of the Upper Palaeolithic at Denisova Cave. *Nature* **565**, 640–644 (2019).

Fowler, C. *et al.* A high-resolution picture of kinship practices in an Early Neolithic tomb. *Nature* **601**, 584–587 (2022).

Meadows, J. *et al.* High-Precision Bayesian Chronological Modeling on a Calibration Plateau: the Niedertiefenbach Gallery Grave. *Radiocarbon* **62**, 1261–1284 (2020).

Sedig, J. W., Olalde, I., Patterson, N., Harney, É. & Reich, D. Combining ancient DNA and radiocarbon dating data to increase chronological accuracy. *J Archaeol Sci* **133**, 105452 (2021).

Miyake, F. *et al.* Verification of the Cosmic-Ray Event in AD 993–994 by Using a Japanese Hinoki Tree. *Radiocarbon* **56**, 1189–1194 (2014).

Oswald, A. *Clay Pipes for the Archaeologist*. vol. 144 (British Series, British Archaeological Reports, 1975).

AlQahtani, S. J., Hector, M. P. & Liversidge, H. M. Brief communication: The London atlas of human tooth development and eruption. *Am J Phys Anthropol* **142**, 481–490 (2010).

Bronk Ramsey, C. Development of the Radiocarbon Calibration Program. *Radiocarbon* **43**, 355–363 (2001).

Reimer, P. J. & Reimer, R. W. A Marine Reservoir Correction Database and On-Line Interface. *Radiocarbon* **43**, 461–463 (2001).

Usoskin, I. G. *et al.* Solar cyclic activity over the last millennium reconstructed from annual ^{14}C data. *A&A* **649**, A141 (2021).

Wu, C.-J., Krivova, N. A., Solanki, S. K. & Usoskin, I. G. Solar total and spectral irradiance reconstruction over the last 9000 years. *A&A* **620**, A120 (2018).

Usoskin, I. G. A history of solar activity over millennia. *Living Rev Sol Phys* **20**, (2023).

Maehara, H. *et al.* Superflares on solar-type stars. *Nature* **485**, 478–481 (2012).

Cliver, E. W., Schrijver, C. J., Shibata, K. & Usoskin, I. G. Extreme solar events. *Living Rev Sol Phys* **19**, 2 (2022).

Hathaway, D. H. The Solar Cycle. *Living Rev Sol Phys* **12**, (2015).

Biswas, A., Karak, B. B., Usoskin, I. & Weisshaar, E. Long-Term Modulation of Solar Cycles. *Space Sci Rev* **219**, 19 (2023).

Adolphi, F. *et al.* Radiocarbon calibration uncertainties during the last deglaciation: Insights from new floating tree-ring chronologies. *Quat Sci Rev* **170**, 98–108 (2017).

Raisbeck, G. M. *et al.* An improved north–south synchronization of ice core records around the 41 kyr ^{10}Be peak. *Climate of the Past* **13**, 217–229 (2017).

Turney, C. S. M. *et al.* High-precision dating and correlation of ice, marine and terrestrial sequences spanning Heinrich Event 3: Testing mechanisms of interhemispheric change using New Zealand ancient kauri (Agathis australis). *Quat Sci Rev* **137**, 126–134 (2016).

95. Wacker, L. *et al.* Findings from an in-Depth Annual Tree-Ring Radiocarbon Intercomparison. *Radiocarbon* **62**, 873–882 (2020).

96. Marcott, S. A. *et al.* Centennial-scale changes in the global carbon cycle during the last deglaciation. *Nature* **514**, 616–619 (2014).

97. Bauska, T. K. *et al.* Carbon isotopes characterize rapid changes in atmospheric carbon dioxide during the last deglaciation. *Proceedings of the National Academy of Sciences* **113**, 3465–3470 (2016).

98. Hogg, A. G. *et al.* Punctuated Shutdown of Atlantic Meridional Overturning Circulation during Greenland Stadial 1. *Sci Rep* **6**, 25902 (2016).

99. Capano, M. *et al.* Onset of the Younger Dryas Recorded with ^{14}C at Annual Resolution in French Subfossil Trees. *Radiocarbon* **62**, 901–918 (2020).

100. Raukunen, O., Usoskin, I., Koldobskiy, S., Kovaltsov, G. & Vainio, R. Annual integral solar proton fluences for 1984-2019. *A&A* **665**, A65 (2022).

101. Oeschger, H., Siegenthaler, U., Schotterer, U. & Gugelmann, A. A box diffusion model to study the carbon dioxide exchange in nature. *Tellus* **27**, 168–192 (1975).

102. Zhang, Q. *et al.* Modelling cosmic radiation events in the tree-ring radiocarbon record. *Proceedings of the Royal Society A: Mathematical, Physical and Engineering Sciences* **478**, 20220497 (2022).

103. Golubenko, K., Rozanov, E., Kovaltsov, G. & Usoskin, I. Zonal Mean Distribution of Cosmogenic Isotope (^{7}Be, ^{10}Be, ^{14}C, and ^{36}Cl) Production in Stratosphere and Troposphere. *Journal of Geophysical Research: Atmospheres* **127**, e2022JD036726 (2022).

104. Zheng, M. *et al.* Modeling Atmospheric Transport of Cosmogenic Radionuclide ^{10}Be Using GEOS-Chem 14.1.1 and ECHAM6.3-HAM2.3: Implications for Solar and Geomagnetic Reconstructions. *Geophys Res Lett* **51**, e2023GL106642 (2024).

105. Roth, R. & Joos, F. A reconstruction of radiocarbon production and total solar irradiance from the Holocene ^{14}C and CO_2 records: implications of data and model uncertainties. *Climate of the Past* **9**, 1879–1909 (2013).

106. Friedlingstein, P. *et al.* Global Carbon Budget 2023. *Earth Syst Sci Data* **15**, 5301–5369 (2023).

107. Ciais, P. *et al.* Five decades of northern land carbon uptake revealed by the interhemispheric CO_2 gradient. *Nature* **568**, 221–225 (2019).

108. Basu, S. *et al.* Estimating US fossil fuel CO_2 emissions from measurements of ^{14}C in atmospheric CO_2. *Proceedings of the National Academy of Sciences* **117**, 13300–13307 (2020).

109. Byrne, B. *et al.* National CO_2 budgets (2015–2020) inferred from atmospheric CO_2 observations in support of the global stocktake. *Earth Syst Sci Data* **15**, 963–1004 (2023).

110. Hua, Q. *et al.* Atmospheric Radiocarbon for the Period 1950–2019. *Radiocarbon* **64**, 723–745 (2022).

121. Delaygue, G., Bekki, S. & Bard, E. Modelling the stratospheric budget of beryllium isotopes. *Tellus B: Chemical and Physical Meteorology* **67**, 1 (2015).

122. Baroni, M., Bard, E., Petit, J.-R., Magand, O. & Bourlès, D. Volcanic and solar activity, and atmospheric circulation influences on cosmogenic ^{10}Be fallout at Vostok and Concordia (Antarctica) over the last 60 years. *Geochim Cosmochim Acta* **75**, 7132–7145 (2011).

123. Panovska, S., Korte, M. & Constable, C. G. One Hundred Thousand Years of Geomagnetic Field Evolution. *Reviews of Geophysics* **57**, 1289–1337 (2019).

124. Green, P. J. & Silverman, B. W. *Nonparametric Regression and Generalized Linear Models: A Roughness Penalty Approach*. (Chapman and Hall/CRC, 1993). doi:10.1201/b15710.

125. Bayliss, A. *et al.* IntCal20 Tree Rings: An Archaeological Swot Analysis. *Radiocarbon* **62**, 1045–1078 (2020).

126. Kromer, B. *et al.* Regional $^{14}CO_2$ Offsets in the Troposphere: Magnitude, Mechanisms, and Consequences. *Science* **294**, 2529–2532 (2001).

127. Manning, S. W. *et al.* Mediterranean radiocarbon offsets and calendar dates for prehistory. *Sci Adv* **6**, eaaz1096 (2020).

128. Kimak, A. & Leuenberger, M. Are carbohydrate storage strategies of trees traceable by early–latewood carbon isotope differences? *Trees* **29**, 859–870 (2015).

129. Scott, E. M., Naysmith, P. & Cook, G. T. Why do we need ^{14}C inter-comparisons?: The Glasgow -^{14}C inter-comparison series, a reflection over 30 years. *Quat Geochronol* **43**, 72–82 (2018).

130. Blackwell, P. G. & Buck, C. E. Estimating radiocarbon calibration curves. *Bayesian Anal* **3**, 225–248 (2008).

131. Geweke, J. Evaluating the Accuracy of Sampling-Based Approaches to the Calculation of Posterior Moments. in *Bayesian Statistics 4* (eds. Bernardo, J. M., Smith, A. F. M., Dawid, A. P. & Berger, J. O.) 169–193 (Oxford University Press, New York, 1992).

132. Brooks, S. P. & Roberts, G. O. Convergence assessment techniques for Markov chain Monte Carlo. *Stat Comput* **8**, 319–335 (1998).

133. Gelman, A. & Rubin, D. B. Inference from Iterative Simulation Using Multiple Sequences. *Statistical Science* **7**, 457–472 (1992).

134. Bronk Ramsey, C. Radiocarbon Calibration and Analysis of Stratigraphy: The OxCal Program. *Radiocarbon* **37**, 425–430 (1995).

135. Geyer, C. J. Markov chain Monte Carlo maximum likelihood. in *Computing Science and Statistics: Proceedings of the 23rd Symposium on the Interface* (ed. Keramidas, E. M.) 156–163 (Interface Foundation, 1991).

136. Robert, C. P. & Casella, G. *Monte Carlo Statistical Methods*. (Springer New York, New York, NY, 2004). doi:10.1007/978-1-4757-4145-2.

127. Heaton, T. J. Non-parametric calibration of multiple related radiocarbon determinations and their calendar age summarisation. *Journal of the Royal Statistical Society Series C* **71**, 1918–1956 (2022).

128. Betancourt, M. A Conceptual Introduction to Hamiltonian Monte Carlo. (2017).

129. Dee, M. W. & Pope, B. J. S. Anchoring historical sequences using a new source of astro-chronological tie-points. *Proceedings of the Royal Society A: Mathematical, Physical and Engineering Sciences* **472**, 20160263 (2016).

130. Weiner, S. *Microarchaeology: Beyond the Visible Archaeological Record*. (Cambridge University Press, Cambridge, 2010). doi:DOI: 10.1017/CBO9780511811210.

131. Waterbolk, H. T. Working with Radiocarbon Dates. *Proceedings of the Prehistoric Society* **37**, 15–33 (1971).

132. Ashmore, P. J. Radiocarbon dating: avoiding errors by avoiding mixed samples. *Antiquity* **73**, 124–130 (1999).

133. McDonald, L. & Manning, S. W. A simulation approach to quantify the parameters and limitations of the radiocarbon wiggle-match dating technique. *Quat Geochronol* **75**, 101423 (2023).

134. Dellaportas, P., Forster, J. J. & Ntzoufras, I. On Bayesian model and variable selection using MCMC. *Stat Comput* **12**, 27–36 (2002).

135. Amaral Turkman, M. A., Paulino, C. D. & Müller, P. *Computational Bayesian Statistics*. (Cambridge University Press, 2019). doi:10.1017/9781108646185.